

Electronic Supplementary Information for: Challenging the Ostwald rule of Stages in Mechanochemical Cocrystallization

Luzia S. Germann,^{a,b,*} Mihails Arhangelskis,^{b,c} Martin Etter,^d Robert E. Dinnebier,^a and Tomislav Friščić^{b,*}

Address:

^a Max Planck Institute for Solid State Research, Heisenbergstr. 1, 70569 Stuttgart (Germany)

^b Department of Chemistry, McGill University, 801 Sherbrooke St. W., H3A 0B8 Montreal (Canada)

Email: luzia.germann@mail.mcgill.ca, tomislav.friscic@mcgill.ca

^c Faculty of Chemistry, University of Warsaw, 1 Pasteura Street, 02-109 Warsaw (Poland)

^d Deutsches Elektronen Synchrotron (DESY), Notkestraße 85, 22607 Hamburg (Germany)

Table of Contents:

Experimental Procedures	2
Materials and Methods	2
Results and Discussion	4
Powder X-ray Diffraction	4
Thermal Analysis	8
Thermodynamic Consideration	9
DFT Calculations	12
Spectroscopic Measurements	13
References	15

Experimental Procedures

1.1 Materials and Methods

Nicotinamide (**nic**), adipic acid (**adi**), acetonitrile (ACN) were all purchased from Sigma-Aldrich and used without further purification. Liquids for dynamic solvent studies were dried with micro sieves, except for acetone, which was dried using K_2CO_3 .

In situ Syntheses

Real-time X-ray powder diffraction (XRPD) monitoring of the mechanochemical syntheses was conducted at the Powder Diffraction and Total Scattering beamline P02.1 at the Deutsches Elektronen-Synchrotron (DESY) in Hamburg using an energy of ca. 60 keV ($\lambda = 0.207 \text{ \AA}$) a modified Retsch MM400 mill operating at 30 Hz.^[1] *In situ* reactions were performed with a total reactant mass of 400 mg, by adding 217 mg (1.48 mmol) adipic acid and 182 mg (1.49 mmol) nicotinamide with 50 μL ACN ($\eta = 0.125 \mu\text{L/mg}$) in a 15 mL poly (methyl methacrylate) (PMMA) milling jar. The reaction was performed using (experiment **A**) two 1.4 g and (experiment **B**) four 1.4 g stainless steel (**ss**) balls, as well as (experiment **C**) two 2.9 g ZrO_2 balls.

Ex situ Syntheses

Form I was synthesized by adding a 1:1 molar ratio of nicotinamide : adipic acid (total reaction mass 400 mg) and 50 μL ACN ($\eta = 0.125 \mu\text{L/mg}$) into a 15 mL PMMA jar with two 1.4 g **ss** balls, and milling at a frequency of 30 Hz for 60 or 90 min.

Form II was synthesized by adding a 1:1 molar ratio of nicotinamide : adipic acid (total reaction mass 400 mg) and 50 μL ACN ($\eta = 0.125 \mu\text{L/mg}$) in a 15 mL stainless steel jar with either one 2.9 g ZrO_2 ball or two 7 mm **ss** balls at a milling frequency of 30 Hz for 90 or 60 min, respectively.

Screening different liquid assisted-grinding additives

182 mg (1.49 mmol) nicotinamide were added with 217 mg (1.49 mmol) adipic acid in either a 15 mL PMMA or a 10 mL Retsch steel jar together with two 7 mm **ss** balls. The mechanochemical reactions were performed by neat (NG) or liquid assisted grinding (LAG) with H_2O , MeOH, ACN, $MeNO_2$ as liquid additive (50 μL , $\eta = 0.125 \mu\text{L/mg}$) using a Retsch MM400 shaker mill for 60 min at 30 Hz.

Postsynthetic Transformation of pure (nic)-(adi) polymorphs

400 mg of presynthesized (**nic**)-(adi) Form I was milled in a 15 mL FTS steel milling jar in the presence of ACN as the LAG additive (50 μL , $\eta = 0.125 \mu\text{L/mg}$) using 2x 7 mm **ss** balls for 60 min at 30 Hz.

400 mg of presynthesized (**nic**)-(adi) Form II was milled in a 15 mL PMMA milling jar in the presence of ACN as the LAG additive (50 μL , $\eta = 0.125 \mu\text{L/mg}$) using 2x 7 mm **ss** balls for 60 min at 30 Hz. After measuring a XRPD pattern, the reaction mixture was milled for another 60 min, adding another 50 μL ACN.

Fourier-Transform Infrared Spectroscopy

Fourier-transform infrared (FT-IR) spectra were measured in attenuated total reflection (ATR) geometry on a PerkinElmer UATR Two, equipped with a diamond crystal. The spectra were background corrected.

Thermal Analysis

Coupled thermogravimetric and differential calorimetric analysis (TGA-DSC) measurements were performed on a Mettler Toledo DTGA/DSC-1 Star Thermogravimetric Analyzer equipped with a horizontal sample stage. Both (**nic**)-(adi) polymorphs were filled into Al_2O_3 crucibles. The experiments were conducted from 30 – 170 – 40 $^\circ\text{C}$ with a heating rate of 5 $^\circ\text{C}/\text{min}$ under an N_2 flow.

Differential Scanning Calorimetry

Differential scanning calorimetry (DSC) experiment was performed with a DSC 214 Polyma from NETZSCH Thermal Analysis and Mettler Toledo DSC-1 Star Thermogravimetric Analyzer. The instruments were calibrated using standard reference materials. The experiments were conducted in an aluminum crucible in the range of 20 – 180 – 20 $^\circ\text{C}$ (11.2 mg sample) with a heating rate of 5 $^\circ\text{C}/\text{min}$ (NETZSCH), and 30 – 170 $^\circ\text{C}$ with a heating rate of 1 $^\circ\text{C}/\text{min}$ (4.68 mg sample) and 5 $^\circ\text{C}/\text{min}$ (4.26 mg sample) on the Mettler Toledo, respectively.

Additionally, three identical DSC measurements of Form I were performed on a DSC2500 (TA instruments Ltd., Delaware, USA), under a stream of nitrogen gas. Three samples (2-3 mg) were placed in lidded but unsealed aluminum pans (with a pinch hole). The three samples of Form I were heated from 25 to 170 $^\circ\text{C}$ with a heating rate of 5 $^\circ\text{C}/\text{min}$ and followed by cooling to RT at rate of 20 $^\circ\text{C}$.

Solid-state Nuclear Magnetic Resonance Spectroscopy

All solid-state nuclear magnetic resonance (ssNMR) spectra were acquired with a Varian VNMRS spectrometer tuned to 100.53 MHz for ^{13}C and 40.51 MHz for ^{15}N . The ^{13}C spectrum of **(nic)·(adi)** Form I was acquired in a 4 mm probe spinning at 13 kHz in 48 scans with a recycle delay of 180 s and a cross-polarization (CP) contact time of 5 ms. The ^{13}C spectrum of **(nic)·(adi)** Form II was acquired in a 7.5 mm probe spinning at 5 kHz using TOSS in 8 scans with a recycle delay of 240 s and a CP contact time of 5 ms. The ^{15}N spectra were acquired in a 7.5 mm probe with spinning at 5 kHz in 360 scans with a recycle delay of 240 s and a CP contact time of 4 ms.

Solvent mediated and long-term stability measurements

A suspension of a physical mixture of **(nic)·(adi)** Form I and Form II with water was filled into a sealed Kapton capillary (\varnothing 1 mm). A XRPD pattern of the suspension was measured after the filling and after 3 days.

To explore the bench stability of both **(nic)·(adi)** polymorphs, XRPD patterns of both forms were measured as synthesized and after storing at ambient conditions for 4 months.

Slurry experiments

Slurry experiments were performed by making 18 different suspensions by putting either Form I or Form II in a closed vial with a total of 9 different liquids (*i*-PrOH, EtOH, H₂O, MeNO₂, ACN, acetone, toluene, hexane, EtOEt) in a Thermo Fisher MaxQ 480R HP incubator (Waltham, MA, USA) set to 20 °C at 90 rpm for about 4 days. XRPD patterns of filtered solids were measured on a Bruker benchtop.

In situ X-ray Powder Diffraction Monitoring and Analysis

2D XRPD patterns were collected with a PerkinElmer XRD1621 (2048 x 2048 pixels). The wavelength was determined with the NIST NSR 660a (LaB₆) standard using two different detector positions to be 0.20744 Å (59.78 keV) for *in situ* XRPD measurements. All 2D XRPD patterns were integrated using either Fit2D or Dioptas.^[2,3]

Sequential Rietveld refinements were performed using TOPAS V5.^[4] A LaB₆ standard measurement was used to describe the instrumental profile function (IPF) by applying equivalent conditions (same milling frequency and exposure time). The IPF was described using $Z/\cos^2(\theta)$ of the Gaussian profile and $X \cdot \tan(\theta)$ of the Lorentzian profile from the modified Thompson-Cox-Hasting pseudo-Voigt function as implemented in TOPAS.

The different crystal structures were obtained from the CSD database {nicotinamide – CSD code NICOAM02; adipic acid – CSD code ADIPAC; **(nic)·(adi)** Form I – CSD code NUKYIC; **(nic)₂·(adi)** – CSD code NUKYOI, **(nic)·(adi)** Form II – solved *ab initio* from XRPD data}. Their microstructure and lattice parameter were refined individually with one *in situ* pattern, where the phase was observed with high abundance and fixed for subsequent sequential Rietveld refinement. During the sequential Rietveld refinement, only the scale parameters of all phases and background were freely refined.

Laboratory and Variable Temperature X-ray Powder Diffraction Experiments

All laboratory (*ex situ* and variable temperature) XRPD measurements were performed on a Stoe Transmission Powder Diffractometer (STADI-P, STOE & CIE) with Cu K α radiation, equipped with an array of three MYTHEN 1K detectors (Dectris Ltd.), and a Ge(111) Johann-type monochromator (STOE & CIE). Samples were filled into 0.5 mm diameter borosilicate (WJM-Glas / Müller GmbH, Germany) or 0.5 mm diameter quartz capillary (Hilgenberg) for low, ambient temperature, and high temperature measurements, respectively. All samples were spun during data collection for better particle statistics.

XRPD measurement for *ab initio* structure determination of **(nic)·(adi)** Form II was performed over a range of 2 – 81.5 ° 2 θ over 16 h using only one single Mythen 1K detector.

All other measurements were performed with an array of the three Mythen 1K detectors from Dectris Ltd. over a range from 0- 55.18 ° 2 θ with 10 min exposure / pattern: High temperature XRPD (HT-XRPD) measurement **(nic)·(adi)** Form I was performed by measuring a XRPD pattern at 20 °C, heating directly to 70 °C and measuring from 70 °C to 120 °C in 2°C steps. The capillary was then cooled to 110 °C and XRPD patterns were collected from 110 – 70 °C in 5°C steps. One last XRPD pattern was collected at 20 °C after cooling.

Low temperature XRPD (LT-XRPD) measurement of **(nic)·(adi)** Form II was conducted in the temperature range of 20 °C down to -180 °C in 10 °C steps ($\Delta T = 6$ °C/min) and then heated directly back to 20 °C.

The XRPD patterns for phase analysis in slurry and milling experiments using different LAG additives were collected using a Bruker D2 Phaser equipped with CuK α radiation and a LYNXEYE linear position sensitive detector (Bruker AXS, Madison, WI). The XRPD patterns were collected in the range of 5 – 40 °2 θ .

Ab initio Structure Determination of polymorph II

Indexing of (nic)-(adi) Form II was carried out by an iterative use of singular value decomposition leading to a monoclinic space group. Systematic absences led to the unique space group $P2_1/c$ with the lattice parameters listed in Table S1. The peak profile was determined by a Pawley refinement using the fundamental parameter approach as implemented in TOPAS. The background was modeled by a Chebyshev polynomial 14th order, with an additional single peak phase at around $21^\circ 2\theta$. The crystal structure of (nic)-(adi) Form II was determined using the global optimization method of simulated annealing. During the *ab initio* structure solution process nicotinamide and adipic acid were described using rigid bodies in z-matrix notation with idealized bond lengths and bond angles, taken from related single crystal structures. Anisotropic peak broadening, most probably caused by some disorder, was modeled by a 4th order spherical harmonics. For the final Rietveld refinement two isotropic thermal displacement parameters, for nicotinamide and one for adipic acid were refined. The background, translation and rotation of the rigid bodies, lattice parameters, and microstructure were freely refined during the final refinement.

Periodic Density Functional Theory calculations

Periodic density functional theory (DFT) calculations were performed using the plane-wave DFT code CASTEP 19.^[5] The input files were created from the CIFs of experimentally determined crystal structures using the program cif2cell.^[6] Calculations were performed with the Perdew–Burke–Ernzerhof PBE^[7] functional supplemented by a many body dispersion (MBD*)^[8–10] correction scheme. The plane wave basis set was truncated at 750 eV cutoff with norm-conserving pseudopotentials used for the core regions of electron density. The 1st electronic Brillouin zone was sampled with a $2\pi \times 0.03 \text{ \AA}^{-1}$ Monkhorst-Pack^[11] k-point grid. The crystal structures were geometry-optimized with respect to atom coordinates and unit cell parameters, subject to the symmetry constraints of the corresponding space groups. The structures were deemed optimized upon reaching the following convergence criteria: maximum energy change $10^{-5} \text{ eV atom}^{-1}$, maximum atomic force 0.01 eV \AA^{-1} , maximum atomic displacement 10^{-3} \AA , residual stress 0.05 GPa.

Results and Discussion

X-ray Powder Diffraction

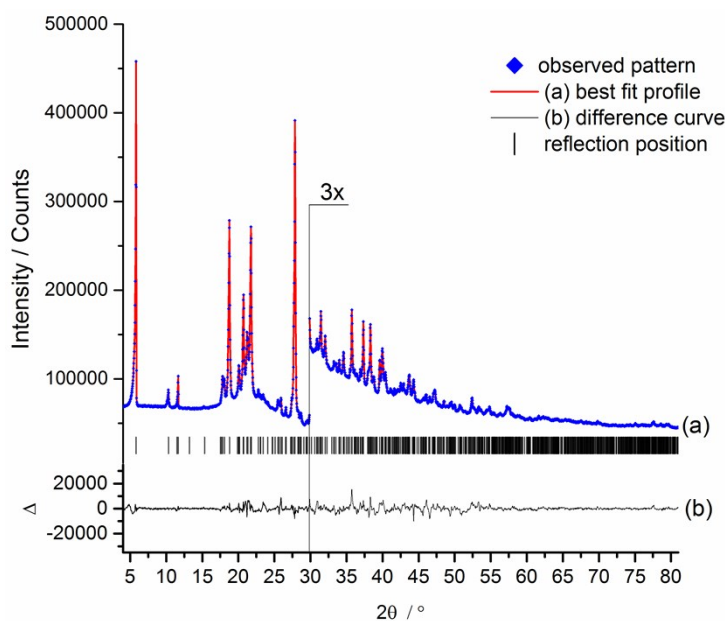


Figure S1: Difference plot of the Rietveld refinement of (nic)-(adi) Form II ($\lambda = \text{CuK}\alpha_1$) with the observed pattern (blue diamonds), calculated pattern (red line), calculated peak positions (dashes), and the difference curve (black line). The higher scattering region ($2\theta > 29.5^\circ$) was enlarged by a factor of 3 for better visualization. The crystal structure has some apparent disorder, visible by anisotropic peak broadening, which was modelled by spherical harmonics (4th order).

Table S1. Crystallographic Information of the Rietveld refinements of **(nic)·(adi)** Form II with selected refinement information.

Polymorph	Form II
Formula	C ₁₂ H ₁₆ N ₂ O ₅
CCDC	1981453
MW / g mol ⁻¹	268.27
Crystal system	Monoclinic
Space group	<i>P</i> 2 ₁ / <i>c</i>
<i>a</i> / Å	4.9815(2)
<i>b</i> / Å	30.3259(19)
<i>c</i> / Å	8.9413(4)
β / °	93.776(4)
<i>V</i> / Å ³	1347.92(10)
<i>Z</i>	4
<i>T</i> / K	295
λ / Å	1347.80(12)
<i>D</i> _{calc} / mg cm ⁻³	1.322
μ / mm ⁻¹	0.878
2 θ range / °	2 - 81.02
No. parameters	50
<i>R</i> _{wp} / % ^[a]	2.74
<i>R</i> _p / % ^[a]	1.86
<i>R</i> _{exp}	0.47
<i>R</i> _{Bragg}	0.99

[a] as defined in TOPAS.^[4]

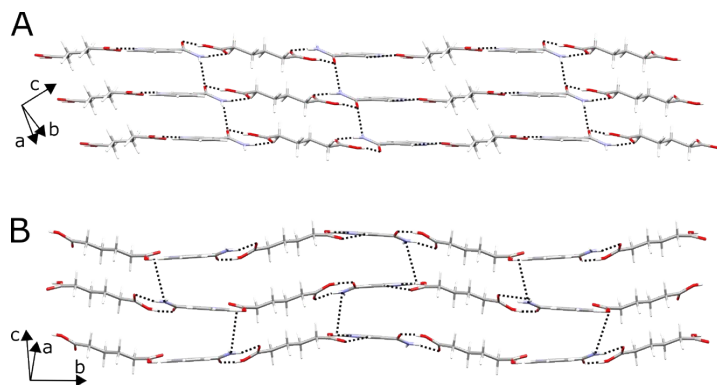


Figure S2: Excerpt of the crystal structures of **(nic)·(adi)** Form I (A) and (B) Form II showing the stacking and interactions between adjacent layers. Hydrogen bonds are represented by black dotted lines.

Milling with different liquid additives

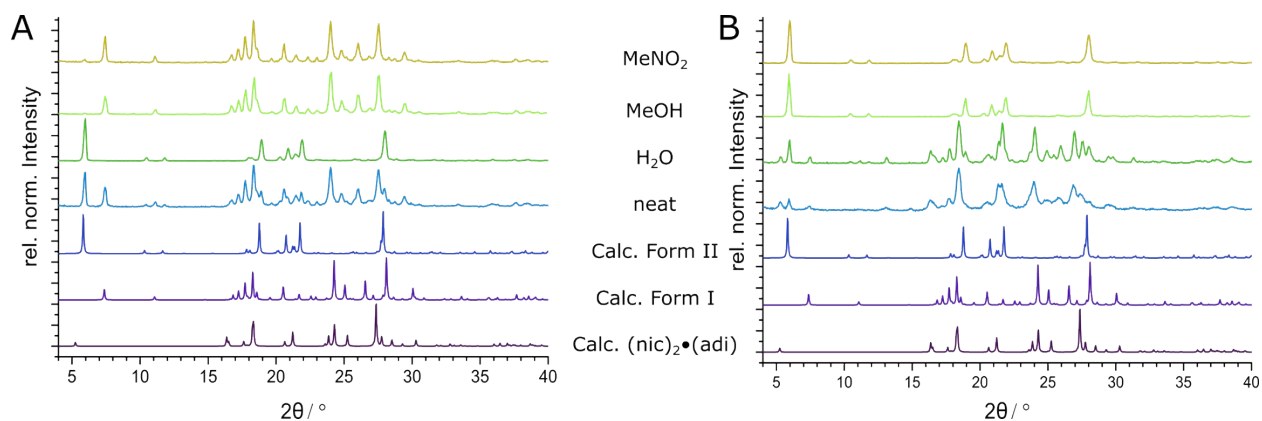


Figure S3: Mechanochemical reactions of (nic)-(adi) cocystals in either (A) PMMA or (B) steel milling jars with otherwise identical reaction conditions ($\eta = 0.125 \mu\text{L}/\text{mg}$, two 7 mm ss balls). From bottom to top: comparison of calculated XRPD patterns of (nic)₂•(adi) - blue, (nic)-(adi) Form I (pink), (nic)-(adi) Form II (black curve) cocystals with experimental XRPD patterns for neat grinding (brown curve), LAG reactions with H₂O (blue grey), MeOH (light blue), ACN (green), and MeNO₂ (green-yellow).

Solvent studies and long-term stability measurement

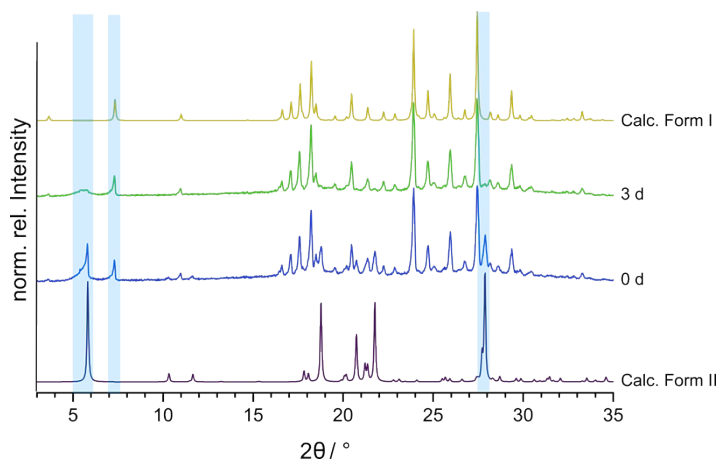


Figure S4: Static solvent-mediated experiments. Comparison of calculated XRPD patterns of (nic)-(adi) Form I (maroon curve) and Form II (black curve) with measured XRPD patterns of a physical mixture of Form I and II after filling into a sealed Kapton capillary ($\phi = 1 \text{ mm}$), filled with water directly after sealing (green curve) and after 3 days (blue curve).

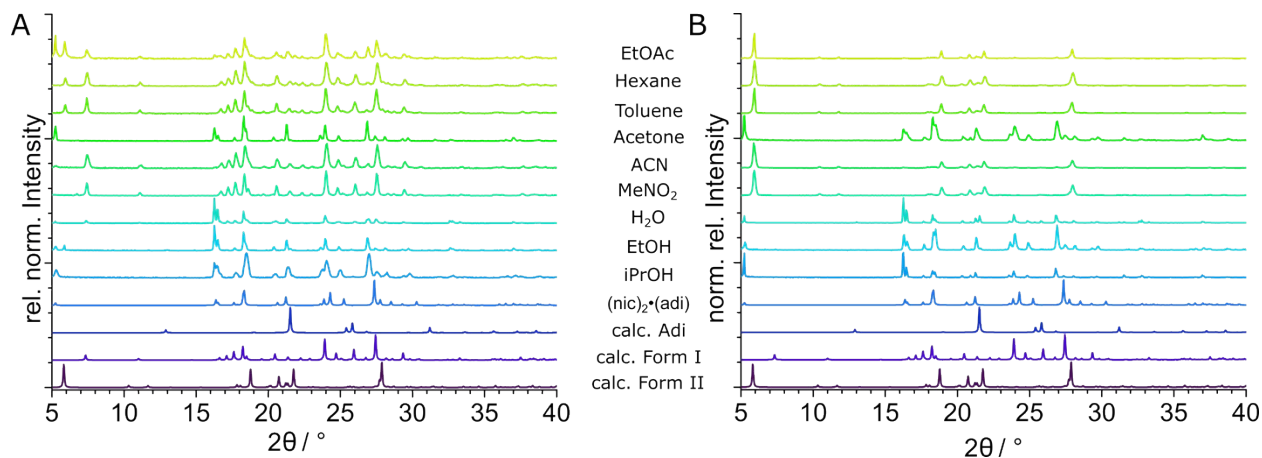


Figure S5: Slurry experiments starting with (A) pure (nic)-(adi) Form I and (B) pure Form II. From bottom to top: Comparison of calculated XRPD patterns of Form II, Form I, adipic acid, and (nic)₂•(adi) with measured XRPD patterns the sample slurries in isopropanol (iPrOH), ethanol (EtOH), water (H₂O), nitromethane (MeNO₂), acetonitrile (ACN), acetone, toluene, hexane, and EtOAc (top).

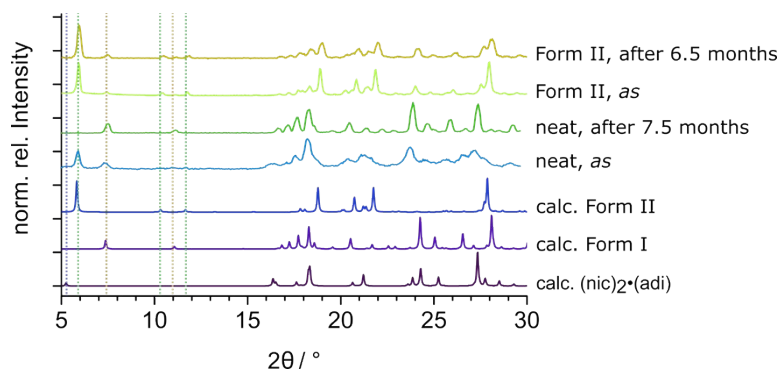


Figure S6: Comparison of calculated and measured PXRD patterns for the second long-term stability evaluation. From bottom to top: calculated PXRD patterns of $(\text{nic})_2 \cdot (\text{adi})$, $(\text{nic}) \cdot (\text{adi})$ – Form I, and $(\text{nic}) \cdot (\text{adi})$ – Form II, measured PXRD patterns of neat grinding (in **ss** jars, milled for 30 mins) measured after synthesis (*as*) and after ca. 7.5 months, Form II as synthesized (*as*) and after ca. 6.5 months. While the reaction mixture from neat grinding in **ss** jars, which lead to formation of $(\text{nic})_2 \cdot (\text{adi})$, $(\text{nic}) \cdot (\text{adi})$ – Form I and II completely transformed into Form I, almost pure Form II transforms much more gradually into Form I. In the top pattern (Form II after ca. 6.5 months) the appearance of diffraction signal of Form I is clearly visible (highlighted by orange dotted points).

Variable temperature PXRD measurements

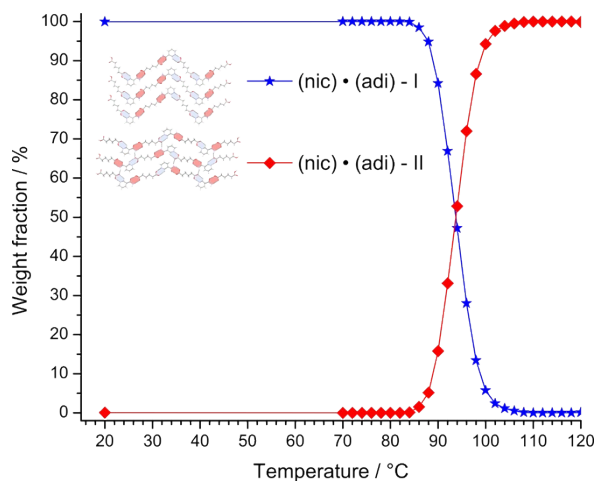


Figure S7: Quantitative phase analysis of the HT-XRPD measurement of $(\text{nic}) \cdot (\text{adi})$ Form I, showing the polymorphic transformation of Form I into II upon heating, starting around 85 °C.

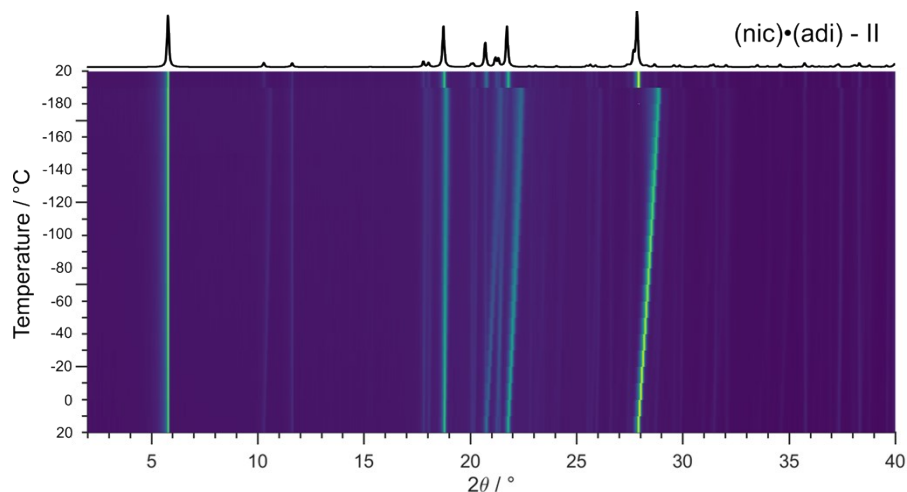


Figure S8: LT- XRPD measurement of **(nic)-(adi)** Form II. The sample was cooled down from 20 to -180 °C and afterwards directly heated up to 20 °C. No phase transformation of **(nic)-(adi)** - Form II into I was observed upon cooling. Calculated XRPD pattern of **(nic)-(adi)** Form II is shown above the 2D plot.

Thermal Analysis

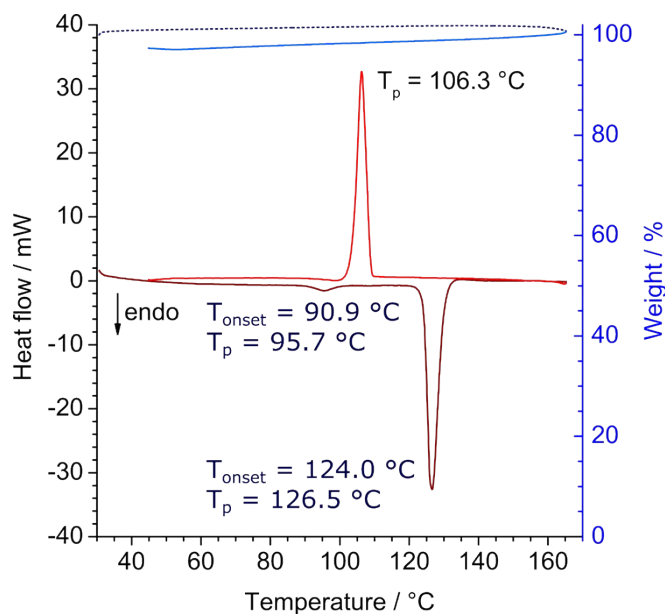


Figure S9: Combined DSC-TGA thermogram of **(nic)-(adi)** Form I measured upon heating (burgundy curve and dotted dark blue) and consequent cooling (red and light blue) with a heating rate of 5 °C/min. Endothermic signals were observed starting at 90.9 and 124.0 °C with peak (T_p) at $T_p = 95.7$ °C and 126.5 °C, respectively, upon heating, corresponding to the polymorphic transition into Form II and melting of Form II, respectively. Crystallisation by cooling was observed at around 106 °C.

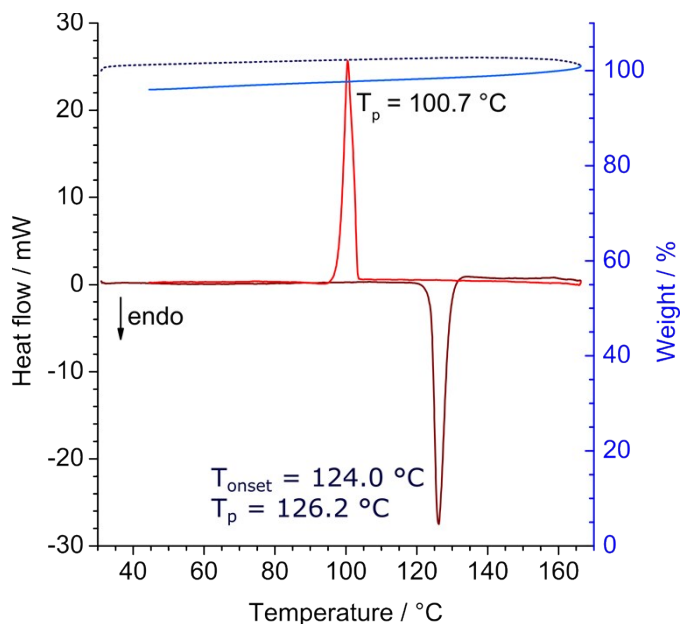


Figure S10: Combined DSC (red)-TG (blue curve) thermogram for **(nic)·(adi)** Form II. An endothermic signal, corresponding to the melting, was observed with an onset at 124 °C and max. peak at 126.5 °C, with crystallization upon cooling occurring at 100.7 °C. Darker colours (burgundy / dotted dark blue) correspond to the heating, red and light blue correspond to the cooling process.

Thermodynamic consideration

In order to calculate the transition enthalpy for conversion of Form I **(nic)·(adi)** into Form II, we integrated the area under the first endothermic signal in the DSC thermograms for **(nic)·(adi)** Form I, which was attributed to the polymorphic transformation of Form I into the high-temperature phase Form II.

Table S2. Transition enthalpy at transition point (T_p) obtained by DSC measurements.

Nr.	Instrument	Heating rate	Integrated area [J/g]	Sample mass [mg]	Transition temperature (T_{onset}) [°C]	Transition enthalpy at T_p [kJ/mol]
Exp. 1	NETZSCH	5 °C/min	5.414	11.2	94.6	1.452
Exp. 2	Mettler Toledo	1 °C/min	5.83	4.68	84.08	1.564
Exp. 3	Mettler Toledo	5 °C/min	6.62	4.26	89.53	1.776

The transition enthalpy at or near room temperature at which the ball milling is conducted was calculated by adding the additional enthalpy required to heat the sample from the temperature of the milling experiment to the onset of transition (T_{onset}). For this purpose, an average milling temperature of ca. 35 °C was assumed, based on temperature measurements of the jar walls after the milling process with an infrared probe, as well as previous reports.^[12] The molar heat capacity ($c_{p,m}$) of **(nic)·(adi)** Form I was calculated from the DSC data for all three measurements with the following formula:

$$c_{p,m} = \frac{\Delta heat\ flow[mW] \cdot \Delta time[s]}{\Delta T[K] \cdot m_{sample}[mg]} \cdot MW$$

with a molecular weight (MW) of 268.26 g·mol⁻¹ for the formula of **(nic)·(adi)**: (C₆H₆N₂O)(C₆H₁₀O₄).

Table S3. Values from experiment 1-3 to calculate the molar heat capacity.

Experiment 1 NETSCH (5 °C/min)			Experiment 2 Mettler Toledo (1°C/min)			Experiment 3 Mettler Toledo (5°C/min)			
Time [s]	T [°C]	Heat flow/mass [mW/mg]	Time [s]	T [°C]	Heat flow [mW]	Time [s]	T [°C]	Heat flow [mW]	
300	40.01548	0.11619	480	38	-0.09264	96	38	-0.52845	
420	50.02052	0.11279	1200	50	-0.09944	240	50	-0.54375	
Difference:	120	10.00504	0.0034	720	12	0.0068	144	12	0.0153

Table S4. Total transition enthalpies ($\Delta H_{\text{trans}}(\text{total})$) derived by combining transition enthalpy at transition point ($\Delta H_{\text{trans}}(T_p)$) and the additional enthalpy (H_{add}) required to heat Form I (nic)·(adi) from 35 °C to the transition point, calculated from the temperature difference (ΔT) and molar heat capacity of Form I ($c_{p,m}$) based on DSC data.

	Experiment 1 NETSCH (5 °C/min)	Experiment 2 Mettler Toledo (1 °C/min)	Experiment 3 Mettler Toledo (5 °C/min)]
$\Delta H_{\text{trans}}(T_p)^{[a]}$ / kJ·mol ⁻¹	1.452	1.564	1.776
$c_{p,m}$ / J·mol ⁻¹ ·K ⁻¹	10.939	23.387	11.562
$\Delta T(T_{\text{onset}}-T_{\text{milling}})^{[b]}$ / °C	59.6	49.08	54.53
$H_{\text{add}}^{[c]}$ / kJ·mol ⁻¹	0.652	1.148	0.630
$\Delta H_{\text{trans}}(\text{total})^{[d]}$ / kJ·mol⁻¹	2.104	1.795	2.406
$\Delta S_{\text{trans}}(T_p)^{[e]}$ / J·mol ⁻¹ K ⁻¹	3.959	4.378	4.897
$\Delta S_{\text{trans}}(35^\circ\text{C})^{[f]}$ / J·mol ⁻¹ K ⁻¹	2.055	0.922	3.013
$\Delta G_{\text{trans}}(35^\circ\text{C})^{[g]}$ / kJ·mol⁻¹	0.818	1.280	0.848

^[a] ΔH at transition point, from Table S2, ^[b] $\Delta T = T_{\text{onset}} - 35^\circ\text{C}$, T_{onset} listed in Table S3; ^[c] $H_{\text{add}} = c_{p,m} \cdot \Delta T(T_{\text{onset}} - T_{\text{milling}})$; ^[d] $\Delta H_{\text{trans}}(\text{total}) = \Delta H_{\text{trans}}(T_p) + \Delta H_{\text{add}}$, ^[e] $\Delta S_{\text{trans}}(T_p) = \Delta H_{\text{trans}}(T_p) / T_p$; ^[f] $\Delta S_{\text{trans}}(T_{\text{milling}}) = \Delta S_{\text{trans}}(T_p) - C_p \ln(T_{\text{onset}} / T_{\text{milling}})$; ^[g] $\Delta G_{\text{trans}}(T_{\text{milling}}) = \Delta H_{\text{trans}}(T_{\text{milling}}) - T \Delta S_{\text{trans}}(T_{\text{milling}})$

The transition enthalpies are **1.6(2) kJ·mol⁻¹** (at transition point temperature, T_p) and **2.1(3) kJ/mol** at 35 °C, which was assumed to be the temperature during milling process. Transition enthalpies were obtained by averaging the transition energies from the three experiments 1-3. The Gibbs free energy of transition is, by definition, zero at transition point temperature, T_p) and **1.0(3) kJ/mol** at 35 °C.

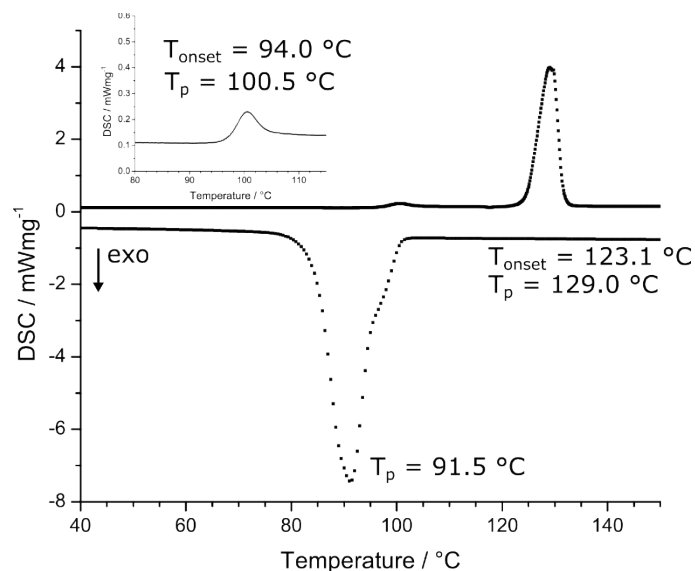


Figure S11: DSC thermogram for (nic)-(adi) Form I (Experiment 1), measured on a DSC 214 Polyma from NETZSCH Thermal Analysis calorimeter, at a heating rate of 5 °C/min in a sealed pan. Endothermic signals were observed at 100.5 °C and 129.2 °C upon heating (top curve), corresponding to the polymorphic transition into Form II and melting of Form II, respectively. Recrystallization of Form II was observed at around 91.5 °C upon cooling (bottom curve).

The DSC thermogram of experiment 2 is shown in the main text, see Figure 6A.

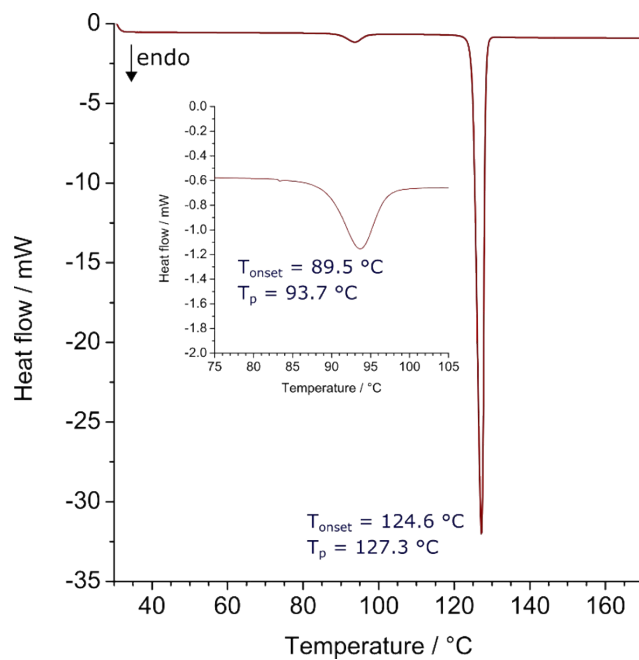


Figure S12: DSC thermogram for (nic)-(adi) - Form I (Experiment 3), measured on a Mettler Toledo DSC-1 Star Thermogravimetric Analyzer, with a heating rate of 5 °C/min in a sealed pan. Endothermic signals were observed at $T_p = 93.7$ °C and 127.3 °C upon heating, corresponding to the polymorphic transition into Form II and subsequent melting of Form II, respectively.

The exact temperature ranges for a polymorphic transformation can vary slightly between HT-XRPD and DSC measurements, due to the intrinsically different nature of both experiments. Whereas DSC measurements are performed continuously, HT-XRPD experiments are performed in a semi-continuous fashion, with alternating heating and measurement modes. This can affect transformation kinetics, as well as transition temperatures.

Reproducibility of phase transition

Three separate DSC measurements of **(nic)·(adi)** Form I (A, B, C) were performed in the range of 25 – 170 °C with a heating rate of 5 °C/min. Transition temperature of the polymorphic transition of Form I into Form II is $T_p = 92.7 \pm 0.1$ °C.

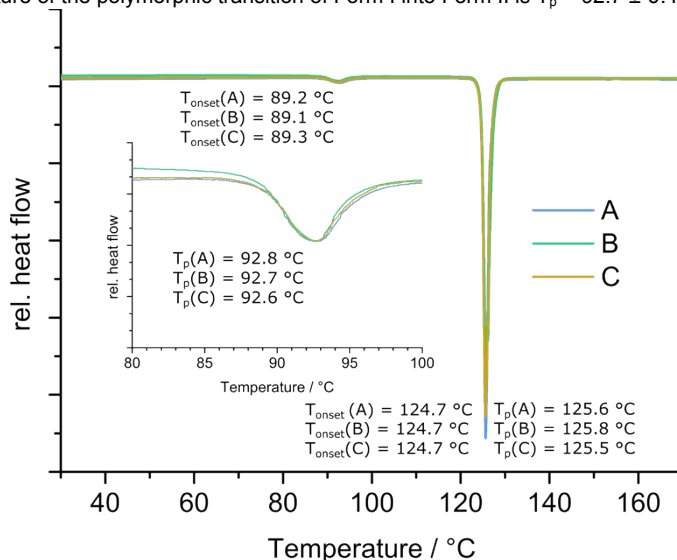


Figure S13: Three separate DSC thermograms for **(nic)·(adi)** - Form I (A, B, C) with an identical heating rate (5 °C/min) measured on a DSC2500 (TA instruments Ltd., Delaware, USA). Endothermic signals were observed at $T_p = 92.1 \pm 0.1$ °C and 125.6 ± 0.2 °C upon heating, corresponding to the polymorphic transition into Form II and subsequent melting of Form II, respectively.

DFT Calculations

Table S5. DFT energies calculated with CASTEP using MBD* corrections.

Structure	CSD refcode	Energy per cell / eV	Energy per formula unit / eV	Energies rel. to starting mix. / kJ·mol ⁻¹
Nicotinamide	NICOAM03	-7985.63	-1996.41	-
Adipic acid	ADIPAC04	-5631.44	-2815.72	-
(nic)·(adi)	NUKYIC	-9624.41	-4812.20	-7.5
(nic)·(adi)	Form II ^[a]	-19248.93	-4812.23	-10.2
(nic)₂·(adi)	NUKYOI	-6808.71	-6808.71	-8.5^[b]

[a] *ab initio* solved from XRPD data, CCDC 1981453. [b] assuming the formation of 0.5 **(nic)₂·(adi)** + 0.5 adi.

Spectroscopic measurement

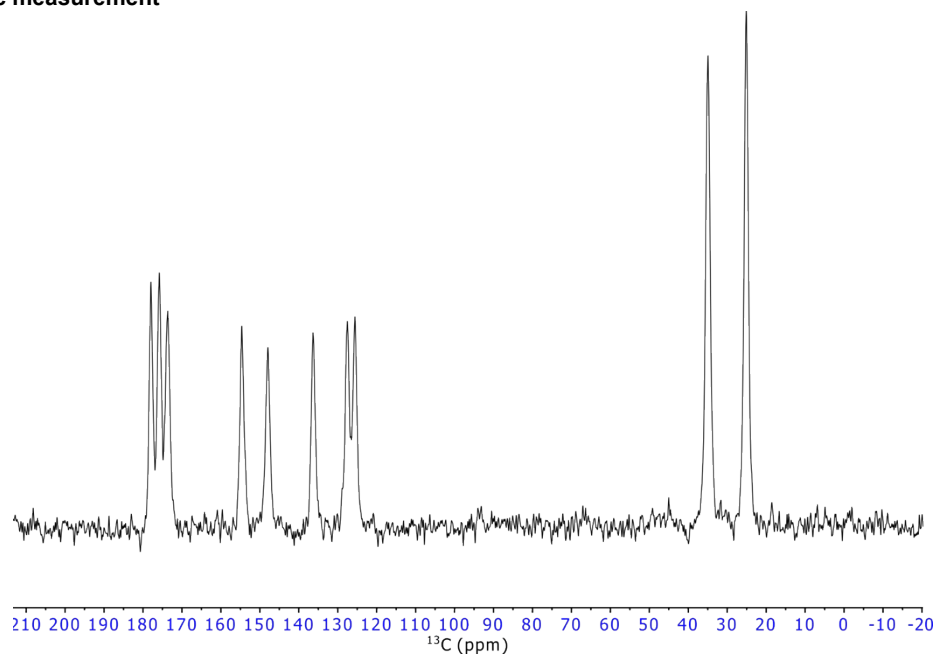


Figure S14: ^{13}C ssNMR spectrum of (nic)-(adi) Form I.

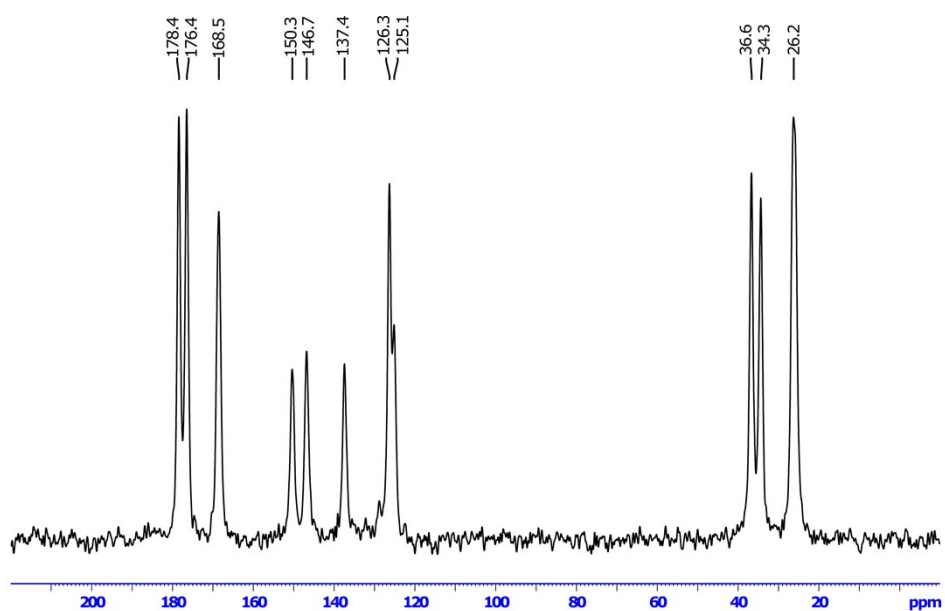


Figure S15. ^{13}C ssNMR spectrum of (nic)-(adi) Form II.

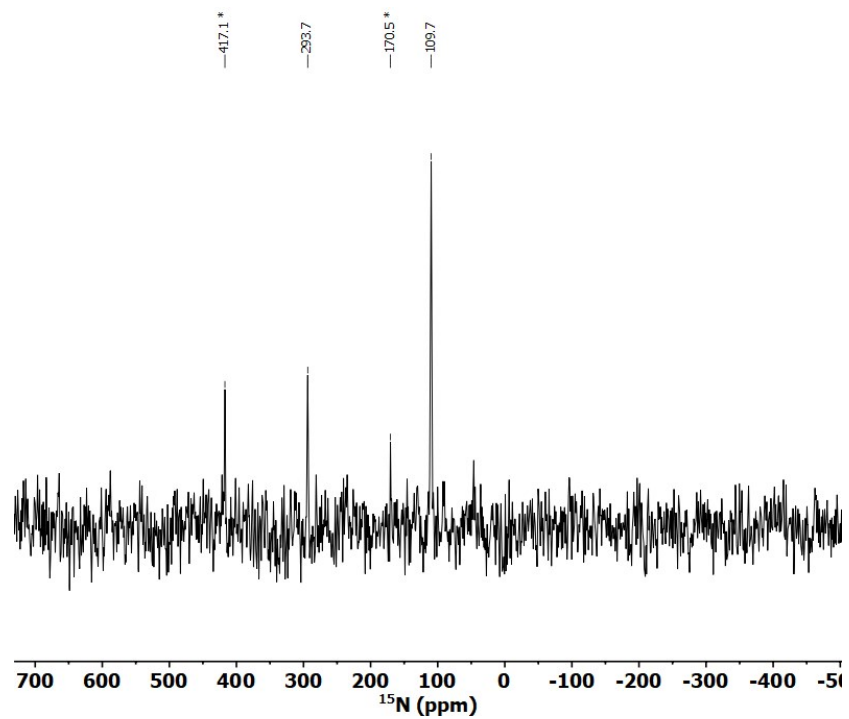


Figure S16: ^{15}N ssNMR spectrum of (nic)-(adi) Form I. Spinning side bands are labelled with an asterisk.

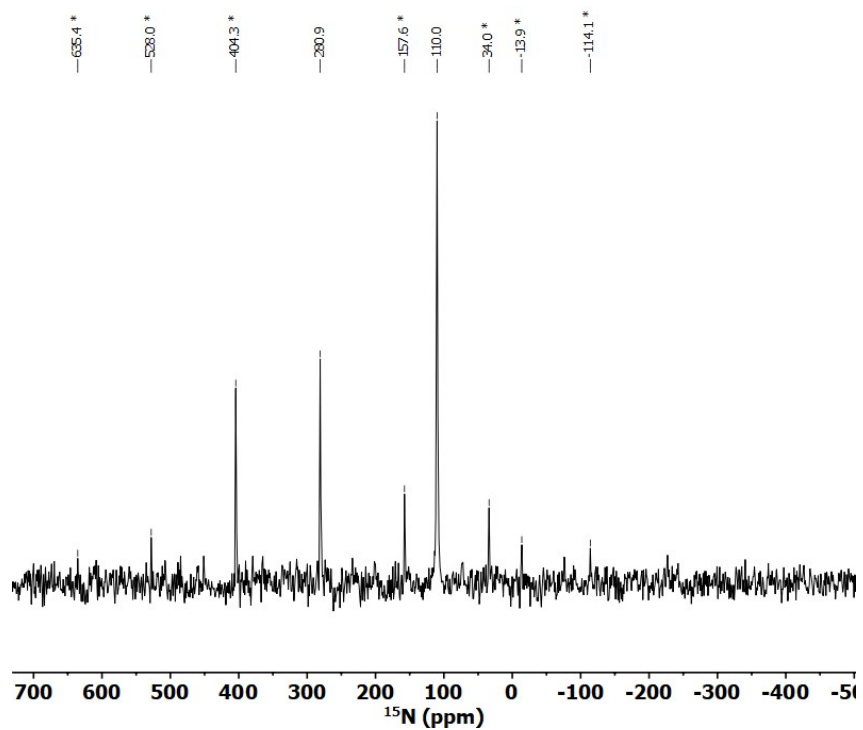


Figure S17: ^{15}N ssNMR spectrum of (nic)-(adi) Form II. Spinning side bands are labelled with an asterisk.

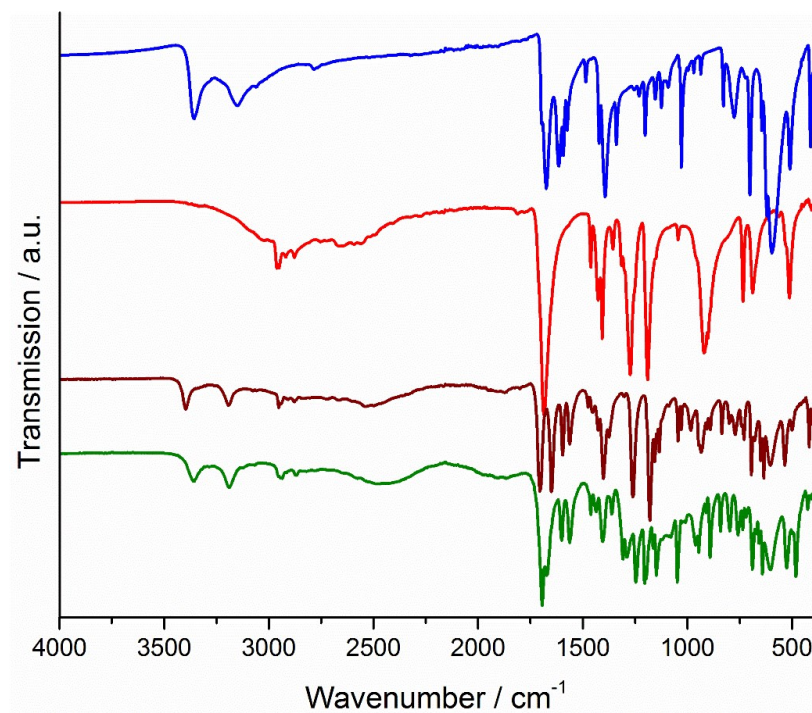


Figure S18: Comparison of FTIR-ATR spectra from (top to bottom) of nicotinamide (blue), adipic acid (red), (nic)-(adi) Form I (burgundy), and (nic)-(adi) Form II (green).

References

- [1] I. Halasz, S. A. J. Kimber, P. J. Beldon, A. M. Belenguer, F. Adams, V. Honkimäki, R. C. Nightingale, R. E. Dinnebier, T. Frišćić, *Nat. Protoc.* **2013**, *8*, 1718–1729.
- [2] A. P. Hammersley, *ESRF Internal Report* **1997**, ESRF97HA02T.
- [3] C. Prescher, V. B. Prakapenka, *High Press. Res.* **2015**, *35*, 223–230.
- [4] A.X.S Bruker, 2014.
- [5] S. J. Clark, M. D. Segall, C. J. Pickard, P. J. Hasnip, M. I. J. Probert, K. Refson, M. C. Payne, *Z. Kristallogr. Cryst. Mater.*, **2005**, *220*, 567-570.
- [6] T. Björkman, *Comput. Phys. Commun.* **2011**, *182*, 1183–1186.
- [7] J. P. Perdew, K. Burke, M. Ernzerhof, *Phys. Rev. Lett.* **1996**, *77*, 3865–3868.
- [8] A. M. Reilly, A. Tkatchenko, *Chem. Sci.* **2015**, *6*, 3289–3301.
- [9] A. Ambrosetti, A. M. Reilly, R. A. DiStasio, A. Tkatchenko, *J. Chem. Phys.* **2014**, *140*, 18A508.
- [10] A. Tkatchenko, R. A. DiStasio, R. Car, M. Scheffler, *Phys. Rev. Lett.* **2012**, *108*, 236402.
- [11] H. J. Monkhorst, J. D. Pack, *Phys. Rev. B* **1976**, *13*, 5188–5192.
- [12] K. Užarević, N. Ferdelji, T. Mrla, P. A Julien, B. Halasz, T. Frišćić, I. Halasz, *Chem. Sci* **2018**, *9*, 2525-2532.